All-SiC Inductively Coupled Charger with Integrated Plug-in and Boost Functionalities for PEV Applications

M. Chinthavali, O. C. Onar, S. L. Campbell, and L. M. Tolbert

Power Electronics and Electric Machinery Group, Oak Ridge National Laboratory, Oak Ridge, TN 37831

chinthavalim@ornl.gov, campbellsl@ornl.gov, onaroc@ornl.gov, tolbertlm@ornl.gov

Abstract— So far, the charging functionality for vehicles has been integrated either into the traction drive system or to the dc-dc converters in plug-in electric vehicles (PEV). This study features a unique way of combining the wired and wireless charging functionalities with vehicle side boost converter and maintaining the isolation to provide a hybrid plug-in and wireless charging solution to the plug-in electric vehicle users. The proposed integrated charger combined with SiC technology shows the end-to-end and dc-to-dc system efficiencies of 85.9% and 88.9% for wireless charging mode, and 88.8% and 92.4% for the wired charging mode of operation.

Keywords—wireless power transfer, on-board charger, integrated charger, wireless charging, boost converter, plug-in electric vehicle charger.

I. INTRODUCTION

With the increased growth in electric vehicles, there is a need for reduction in weight, size, and cost while increasing the efficiency and power rating of the on-board chargers (OBCs). Integrating the function of charging into the traction drive systems of PEVs has been proven to significantly reduce the volume and weight and increase the power density of the of OBCs [1]-[6]. Since all the components are on-board, the power levels are typically limited because of the size and weight constraints on the vehicle; therefore, charging times are usually long. Higher power levels can be achieved with off-board chargers; however, both the on-board and off-board chargers featuring plug-in options inherently pose a danger of electric shock. Furthermore, depending on the plug and cable ratings, they are heavy and inconvenient. Additionally, there is always a possibility of forgetting to plug-in and running out of charge.

Some of the challenges associated with plug-in chargers can be eliminated by implementing wireless power transfer (WPT) technology. WPT is a safe, convenient and flexible charging method for PEVs. However, having the wired (plug-in) and wireless charging systems available at the same time is critical, especially before the wireless charging infrastructure is readily available. Along with convenience, the other aspects

of the charging technology that need to be addressed are the cost and the efficiency of the charger.

Integrated chargers generally will provide huge cost benefits by utilizing same components for different functionalities. By integrating vehicle side components with wireless charging functionalities, substantial cost benefits can be achieved [7], [8]. In this integration, multi-functional operations can be achieved since charging and boost modes of operation are independent. However, because of the high number of power conversion states, the other challenge for wireless integrated topologies is the total system efficiency. According to the Society of Automotive Engineers (SAE) J2954 standard development activity [9], greater than 85% efficiency is expected from utility outlet to the vehicle high voltage (HV) bus in wireless charging applications. Currently, silicon (Si) based devices, comprised mostly of integrated gate bipolar transistors (IGBTs) and PiN diodes, are being used in charging and traction drive systems. With the limitations of Si based technology, it becomes extremely difficult to achieve the desired efficiency, especially at higher frequencies and power levels. WBG device technology with lower losses and higher operating temperature can be utilized to address this issue and prove to be a vital solution for the wireless charging technology.

It is evident, from the literature survey, that the topologies with integrated dc-dc converter and charging functionality have no isolation in the system [1]-[6], [10]-[19]. Isolation is an important feature that is required for user interface systems that have grid connections to prevent potential shock hazards and also ground faults and therefore isolation is a major limitation that needs to be addressed along with the integrated functionality. There are two solutions that can be used to essentially address this issue. One is a traditional high frequency (HF) isolation transformer that can be added to the integrated system on board. However, this adds an additional power stage, complexity, component cost, and weight to the car, and minimizes the impact of the integrated functionality. The other solution that can be utilized is an inherently isolated wireless charging system that can provide the required isolation from the grid. The WPT system has a significant benefit compared to other systems in terms of the component count that can be added to the car. The secondary system in the car can be as simple as a LC resonant coil with a rectifier and a filter capacitor. The rest of the system is located on the grid side stationary unit that has several stages of power conversion. Both the above-mentioned solutions are very attractive and have their pros and cons. However, there is a

unique way of combining these functionalities and providing the best solution to EV and PHEV users. The topology proposed in this study integrates the wireless charging system and the boost converter of the traction drive system while moving the high frequency isolation stage off-board in addition to the inherent airgap. This architecture has two levels of isolation with multifunctional operation flexibility, such as charging and boosting function. The proposed system also utlizes Silicon carbide devices to improve the overall efficieny and makes the system more comparable with on-board charger systems efficiencies in a commercial EVs. The overall system architecture and the details of the design trade-offs compared to an on-board charging system are discussed in the following sections.

II. System Description

Figure 1 illustrates the integrated stationary wireless charging circuit topology that is proposed. The topology has five stages of power conversion from the wall to the vehicle battery in the wireless charging mode and four stages in the wired charging mode. The boost mode of operation essentially remains the same as it is in the on-road vehicles.

A. Wireless Charging Mode of Operation

Figure 2 demonstrates the circuit topology for the wireless mode of operation. Utility ac power is converted to controllable dc voltage by the active front-end rectifier with power factor correction (PFC). Adjustable dc voltage is applied to the input of the high frequency (HF) full-bridge inverter with a controlled duty ratio. The HF stage delivers excitation current to a series tuned primary coil for magnetic field generation that is linked to the secondary coil on the vehicle across the air gap. Voltage induced at the secondary is rectified, filtered, and delivered to the vehicle HV battery. The integrated wireless charger has an advantage compared to the conventional topology. The boost inductor in series with the battery pack will minimize the battery current ripples, and with the capacitor, it acts as a low pass filter. This feature will increase the reliability and the lifetime of the battery. WPT applications may require inclusion of a HF transformer to provide electrical isolation of the WPT primary pad and cabling from the utility. Isolation requirements and grid power quality are currently being discussed by SAE J2954 standards development committee [9]. In addition to the isolation, the HF transformer can be utilized to step down the HF inverter output voltage that enables the inverter to be operated at high voltage and low currents and results in higher efficiencies for the system.

B. Wired Charging Mode of Operation

The HF transformer solution also provides the flexibility of using the system as a wired charger. This can be achieved by simply using a relay system that can be operated to disconnect the resonant coil system and connect the output of the HF transformer to the on-board section of the integrated charger system. The wired charging mode of operation has four power conversion stages. This mode of operation will enable the EV users to use the plug-in charger wherever there is no wireless charging option. The efficiency of the system is compared to the wireless mode of operation in Section VI. Figure 2 shows the circuit topology for the wireless mode of operation.

C. Boost Mode of Operation

The boost mode operation simply utilizes a single stage switch and a diode combined with an inductor designed for boost operation. The wireless and wired charging power stages are completely isolated by using the relays in the system. This topology is completely based on the two independent functions of the integrated systems, (1) charging and (2) boost, which do not require simultaneous operation as shown in Fig. 4.

III. Simulations of the Proposed System

A simulation model was built using PSIM which is an implementation of the overall system depicted in Fig. 1. The resonant coil system is modeled as a loosely coupled transformer model. The HF transformer is modeled as an ideal transformer with series leakage inductance. The magnetizing branch inductance, L_m, is assumed to be too high for this highly coupled core based HF transformer and therefore has not been included in the model. The control system that was implemented for this model is discussed in detail in [20], [21]. The only difference is the addition of the transformer model which affects the controller gains. The parameters used for the simulation are shown in Table I. The inductances of the coils were obtained from the measured values of the prototypes built. The turns-ratio of the transformer is designed to be 10:2. This was enough to step the voltage of the inverter output and accommodate the designed resonant system gain of 3.1 at 22 kHz. This turns ratio also enabled control over a wide range of power and a boost voltage of up to 600 V max.

A. Wireless Charging Mode of Operation

Figures 5 and 6 show the complete system response to a 6.6 kW charge power request at the battery terminals. The current that the controlled rectifier draws from the grid is in phase with the grid voltage with close to unity power factor. The reference and actual measured grid current waveforms are plotted in Fig. 5 (a) in order to demonstrate the performance of the current control loop.
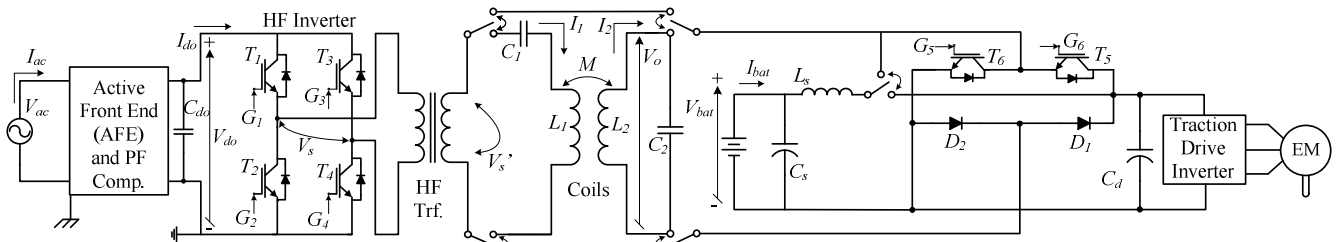

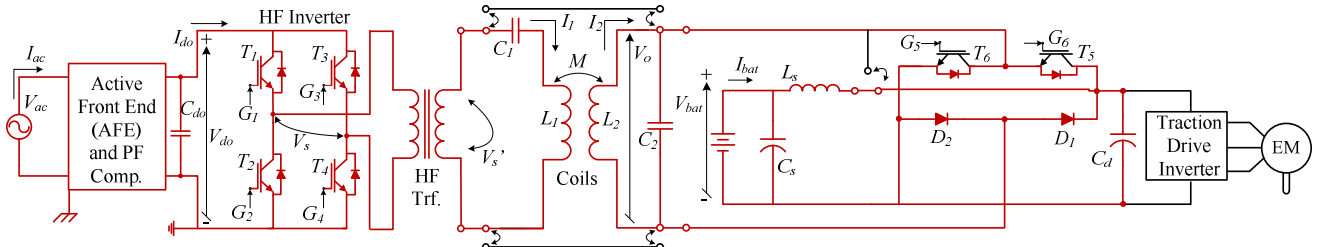Fig. 1. Circuit architecture of the proposed integrated charger.

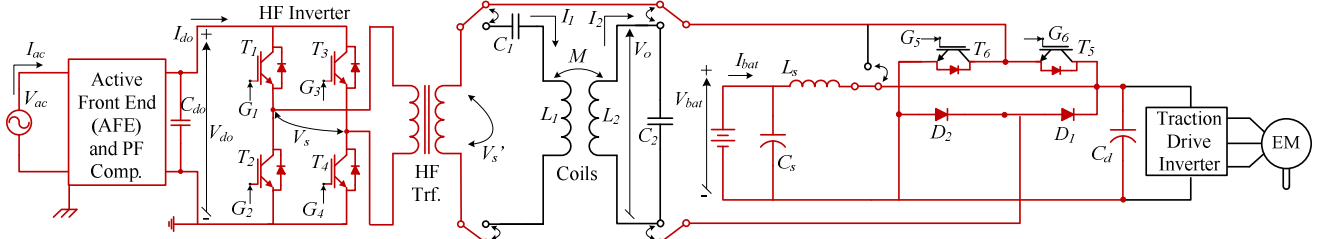Fig. 2. Circuit configuration for wireless operation mode.

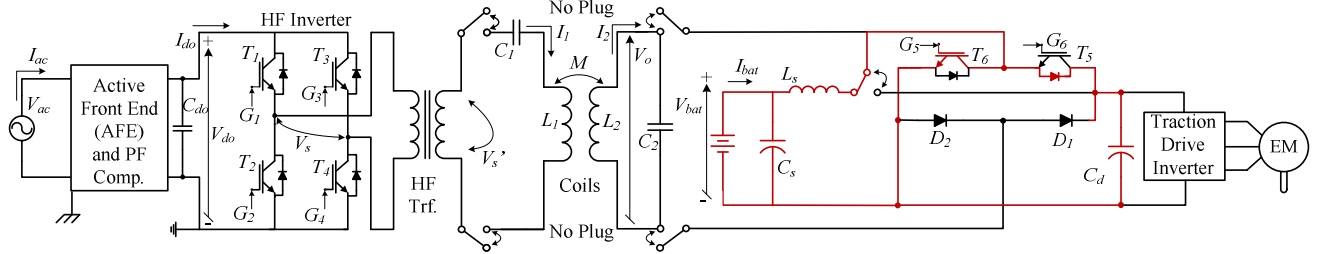Fig. 3. Circuit configuration for wired operation mode.

Fig. 4. Circuit configuration for boost mode of operation.

In order to supply this amount of power, the control system automatically boosts and regulates the dc-link voltage to ~450V as shown in Fig. 5 (b). The inverter output voltage, primary coil voltage, and the transformer output voltage in Fig. 6 (a) and (b) show the impact of the total transformer leakage inductance. The voltage has a transient curve because of the drop across the leakage inductance and the RMS value of the voltage across the coil is reduced. The battery voltage and battery current with detailed zoom show the resulting ripples in Fig. 6 (c). Figure 6 (c) also shows the amount of power transfer to the load side (~6.6kW).

TABLE I. SIMULATION MODEL PARAMETERS

| Parameter	Symbol	Value	Unit
AC input voltage	V_{ac}	220	[V_{ac}]
DC link voltage	V_{do}	350-600 (controlled)	[V_{dc}]
Primary tuning capacitor	C_1	0.45	[μF]
Primary coil inductance	L_1	115.79	[μH]
L_1 internal resistance	R_{L1}	122.7	[$m\Omega$]
Secondary coil inductance	L_2	132.6	[μH]
L_2 internal resistance	R_{L2}	150.8	[$m\Omega$]
Secondary tuning capacitor	C_2	0.40	[μF]
Coupling factor	k	0.23	#
Distance between the coils	z	160	[mm]
Filtering capacitor	C_o	680	[μF]
Battery nominal voltage	V_b	310	[V_{dc}]
Battery target power	P_b	6600 (target)	[W]

(a)

(b)
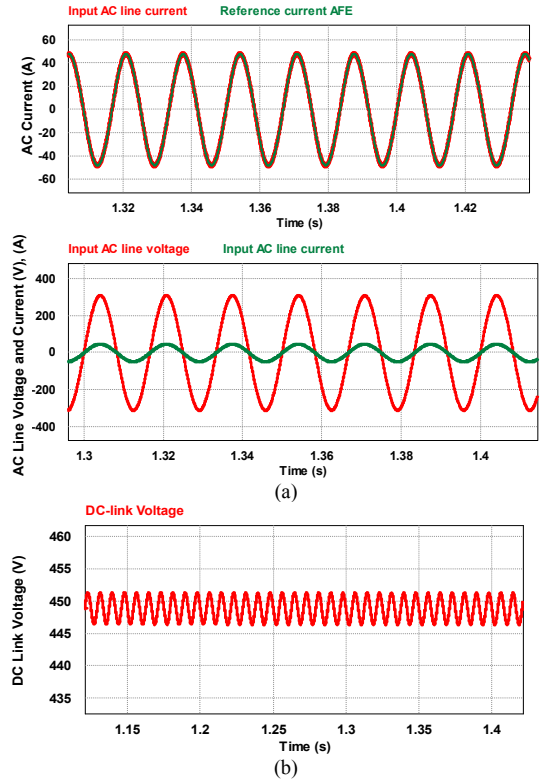
Fig. 5. Simulation result: AC line voltage and current (a) and the boosted DC link voltage (b).

1309
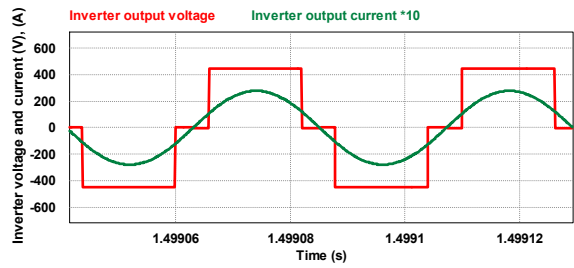
(a)
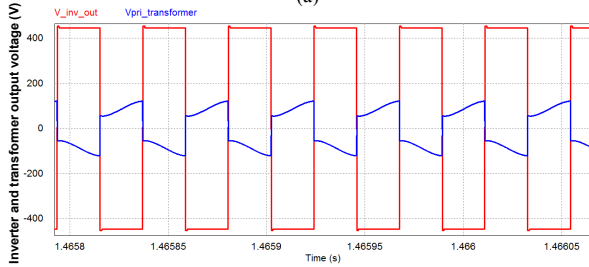
(b)
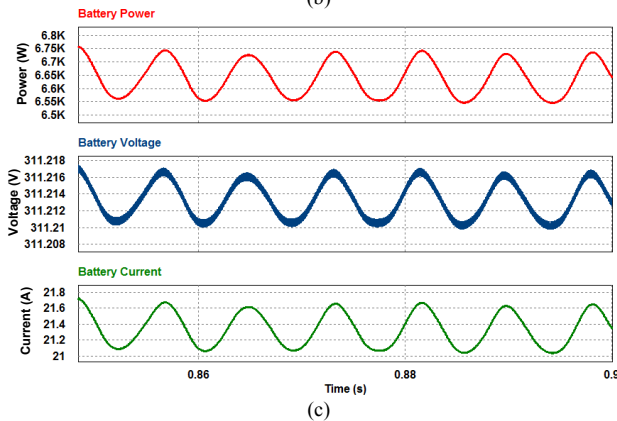
(c)

Fig. 6. Simulation results: Inverter output voltage and current (a), inverter output voltage and primary coil voltage (transformer output) (b), vehicle battery power, voltage and current (c) waveforms.

B. Wired Charging Mode of Operation

The wired mode was simulated without the resonant tank and the parameters of the components except the transformer were kept the same. The turns ratio of the transformer was changed to 8:5 to account for the abesnce in the resonant gain and the corresponding design parameters were used.
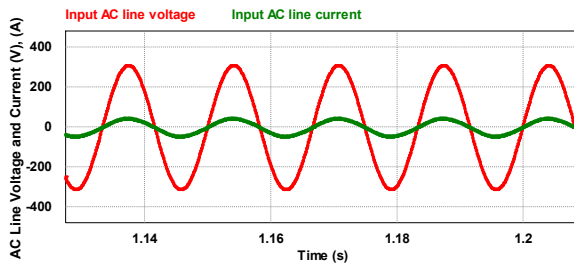

Fig. 7. Wired mode simulation results showing grid voltage and current.

The control system strategy for the wired mode was kept the same. Unity power factor is achieved with the wired mode as well. AC line grid voltage and current are plotted in Fig. 7 whereas Fig. 8 shows the DC link voltage without coils. It is seen from Fig. 8 that the rectfied boosted voltage is higher

than that of the wireless mode. This is due to the fact that system requires higher voltage since there is no resonating circuit after the inverter and there is no resonant voltage gain and therefore a higher voltage level is needed for the same level of power transfer to the load. The inverter and the transformer output voltages and currents are shown in Fig. 9. Finally, Fig. 10 shows the amount of power transfer to the load side (~6.6 kW). Again this verifies that the closed loop control system is working and the output power is regulated to the designed value.
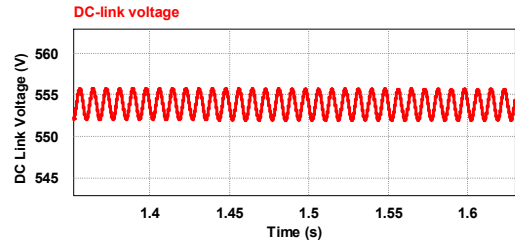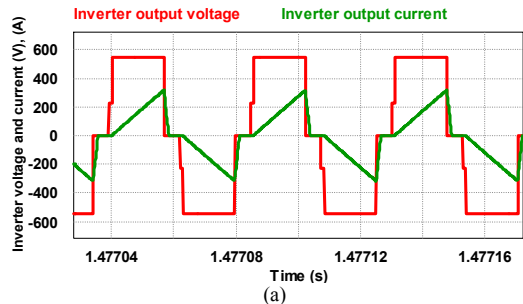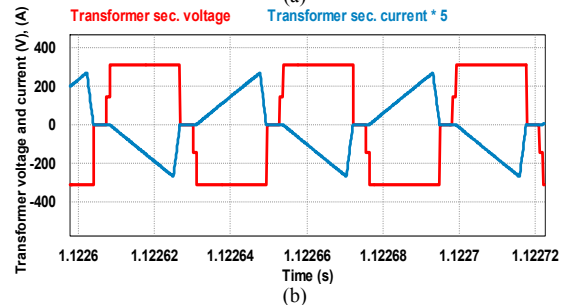

Fig. 8. DC link voltage in wired mode of operation.

(a)

(b)

Fig. 9. Inverter output voltage and current (a) and transformer output voltage and current (b).
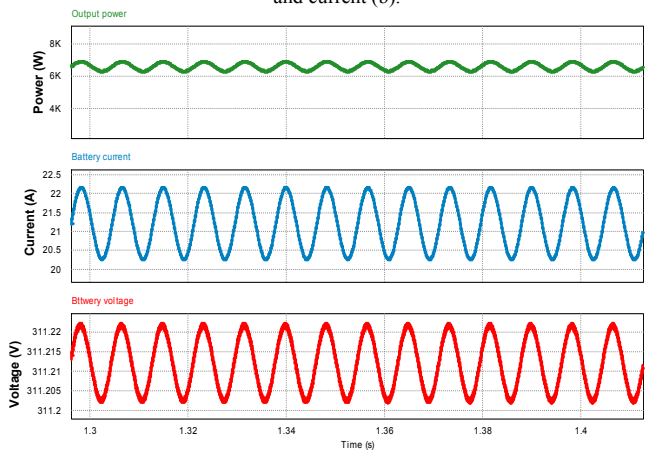

Fig. 10. Battery power, current, and voltage under wired mode.

IV. EXPERIMENTAL TEST SETUP AND RESULTS

The active front-end rectifier was built using the commercially available 1200V, 100A SiC MOSFET-based phase-leg modules. The SiC modules were used because of the high voltage in the dc-link. The details of the design are presented in [20]. The HF inverter was built using the same SiC devices. Also, vehicle side rectifier consist of the internal SiC diodes of these devices The inverter and the PFC were cooled using a water ethylene glycol mix and the receiver side rectifier was cooled using fan based heat sink. The control system of the inverter is implemented within a TMS320F28335PGFA DSP module from Texas Instruments. The primary side (grid-side) power stage is given in Fig. 11, including the front-end rectifier (a) and the HF inverter (b). The experimental setup of the system with SiC-based active-rectifier including primary (bottom) and secondary coil (top) and in the background the HF transformer, resonant tuning capacitors and vehicle side rectifier with a small filter capacitor are shown in Fig. 12 (a) and (b).
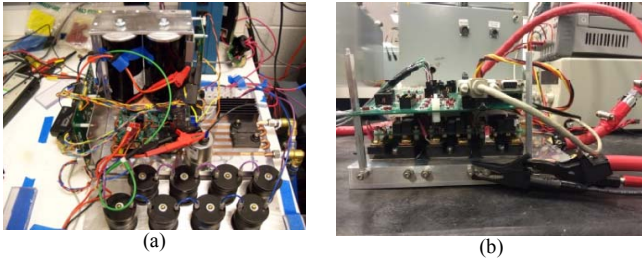

(a)   (b)

Fig. 11. SiC-based active front-end rectifier with PFC (a) and the SiC. H-bridge inverter (b).

A. Wireless Mode of Operation Experimental Results

The experimental set-up was used to evaluate the wireless mode first. The transformer was wound for a turns-ratio of 10:2 as per the design and the load voltage was set to 311 V_{dc}. The ac input voltage was ramped up to 220 V_{rms} and the corresponding power to the load was recorded. The required power output was changed in steps and the efficiencies were calculated. The desired 6.56 kW power transfer to the vehicle battery for an input power of 7.63 kW to the system was achieved. This power level corresponds to ~85.9% overall efficiency from AC grid to the vehicle battery terminals. The voltage and current waveforms for the AC input and DC link to the inverter are given in Fig. 13 whereas the inverter, transformer, coil, and rectifier output waveforms are given in Fig. 14. The detailed stage-by-stage power flow of the system is illustrated in Fig. 15 (highlighted with frame).

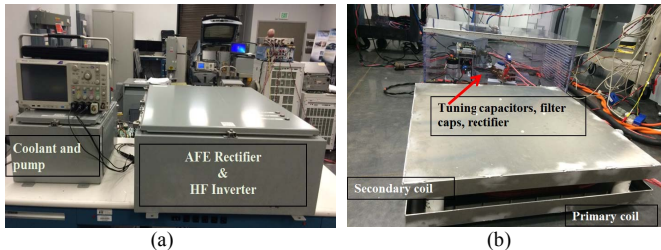(a)   (b)

Fig. 12. Experimental test setup: PFC converter integrated with the high frequency power inverter and enclosed in the stationary box with the cooler (a) and primary and secondary coils, tuning capacitors, and vehicle side rectifier and filter (b).
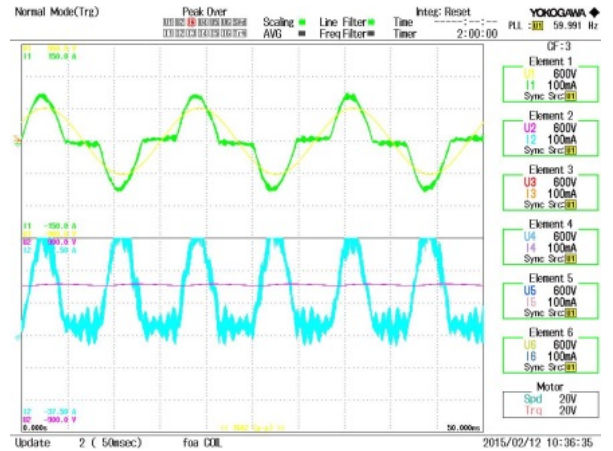

Fig. 13. Experimental voltage and current waveforms for the AC input and the DC link to the inverter.
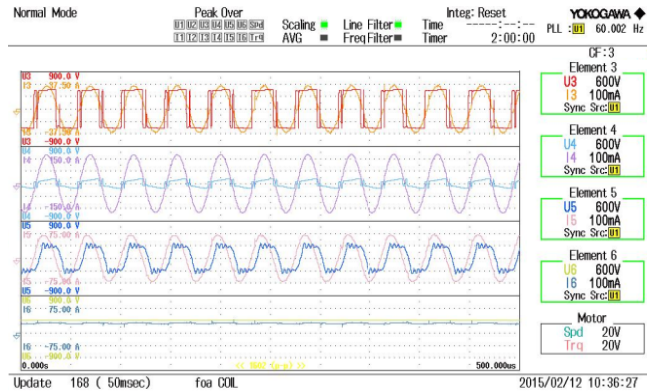

Fig. 14. Experimental voltage and current waveforms for the inverter, transformer, coil, and rectifier outputs.
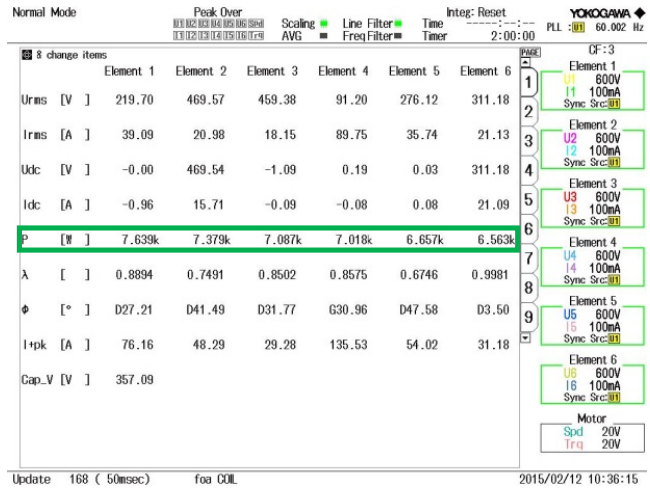
Fig. 15. The stage-by-stage power of the system after each power conversion.

There are several important parameters that can be analyzed to understand the impact of each component and also to validate the simulation results. The dc-link boost voltage is 459 V_{dc} which closely matches with the simulated value of 452 V_{dc} for the same system parameters. One more important parameter is the leakage inductance of the transformer and its effect on the turns-ratio. The turns-ratio from the experiments is 10:2, validating the designed value. This turns-ratio although is an

expected value for the design, the resonant tank load makes the parameters in the transformer more critical. The most important parameter is the leakage inductance and the turns-ratio associated with that design which will make the voltage drop across the leakage inductance. This will affect the RMS value of the voltage on the secondary side. So for this design the turns-ratio being close shows that voltage-drop across the leakage inductance for the transformer is negligible. This can also be observed in the waveforms of the transformer secondary voltage as shown in Fig. 14. The value of leakage inductance is 45 μH and the current is around 18 A_{rms}. The inductive reactance is dependent on the resonant frequency. So for higher frequencies the voltage drop could be even higher which makes the impact of the transformer parameters even more critical. As shown in Fig. 15, stage by stage cascaded efficiencies are found as follows: Active front-end rectifier: 96.6%, inverter: 96%, transformer: 99%, coils: 94.9%, and rectifier: 98.6%. This results in 85.9% end-to-end efficiency and 88.9% dc-to-dc efficiency in wireless charging mode. The proposed system is also tested at different power levels; i.e., at 0.93, 2.35, 3.21, 4.01, 4.79, 5.54, 6.28, 6.56 kW, and the efficiency of the each power conversion stage is obtained with respect to the different levels of the charging power delivered to the load. The efficiency vs. power curves of the PFC, inverter, coils, and the rectifier are presented in Fig. 16 (a) and (b).

(a)

(b)
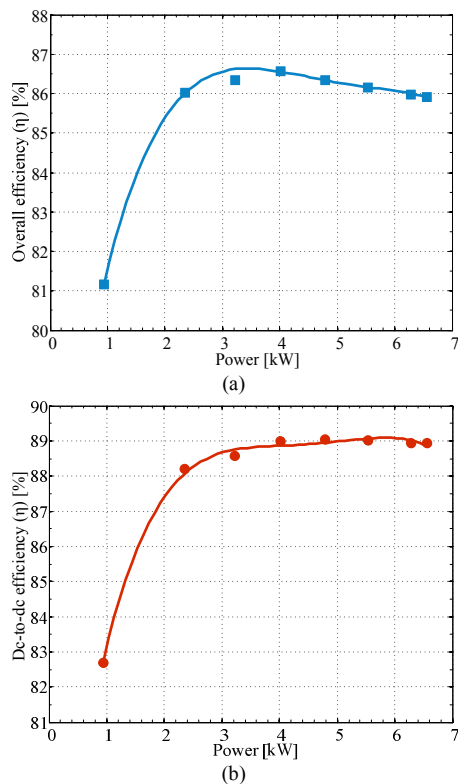
Fig. 16. System efficiency at different power transfer levels for wireless operation: (a) Overal efficiency and (b) dc-to-dc efficiency.

B. Wired Mode of Operation Experimental Results

The experimental set-up that was used to evaluate the wireless mode was changed to the wired mode test by changing the transformer and removing the resonant network. The transformer was wound for a turns-ratio of 8:5 as per the design and the load voltage was set to 311 V_{dc}. The ac input voltage was ramped up to 220 V_{rms} and the required power output was changed in steps. The dc-link boost voltage is 555.76 V_{dc} which closely matches with the simulated value of 554 V_{dc} for the same system parameters. Unlike the wireless mode of operation the effect of leakage inductance is negligible. The desired 6.7 kW power transfer to the vehicle battery for an input power of 7.58 kW to the system was achieved. This power level corresponds to ~88.76% overall efficiency from AC grid to the vehicle battery terminals. The detailed stage-by-stage power output of the system is illustrated in Fig. 17. The voltage and current waveforms for the AC input and DC link to the inverter are given in Fig. 18, whereas the inverter, transformer, coil, and rectifier output waveforms are given in Fig. 19.
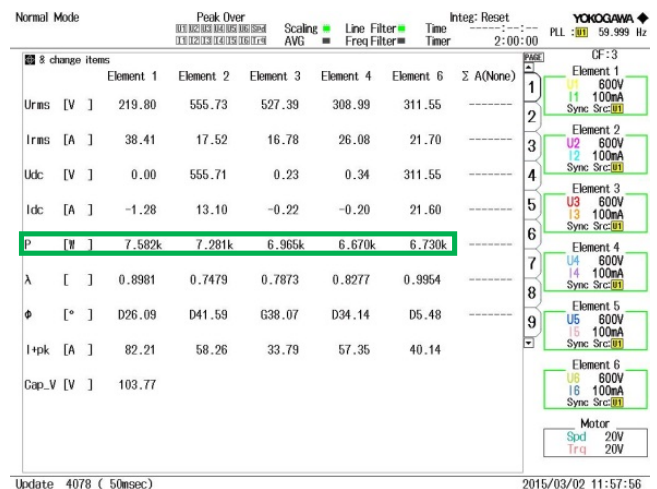

Fig. 17. Detailed stage-by-stage powers of the wired charging operation mode.
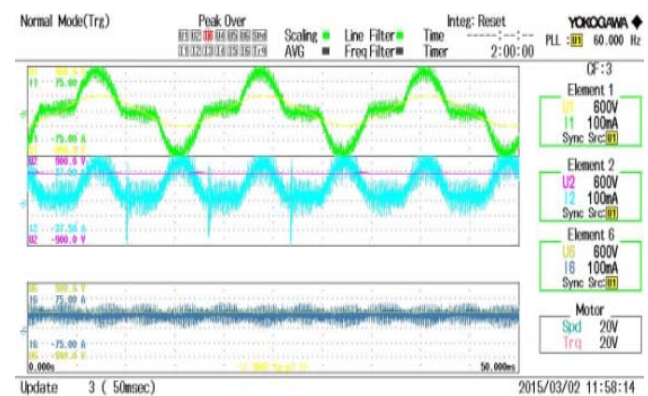
Fig. 18. Experimental voltage and current waveforms for the AC input and DC link to the inverter.

According to Fig. 17, dc-to-dc (from inverter input to the vehicle battery) and the overall end-to-end efficiency values of each power conversion stages are as follows: active front-end rectifier: 96%, inverter: 95.7%, transformer: 97.6%, rectifier: 99%. The proposed system is also tested at different power levels; i.e., 1.42, 2.29, 3.24, 4.03, 5.6, and 6.73 kW and the efficiency of the each power conversion stage is obtained with

respect to the different levels of the charging power delivered to the load, as shown in Fig. 20 (a) and (b).

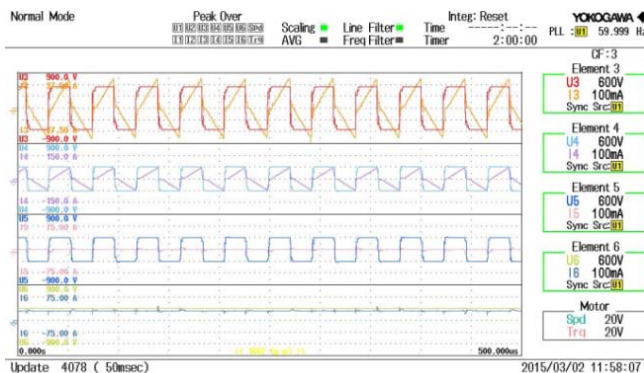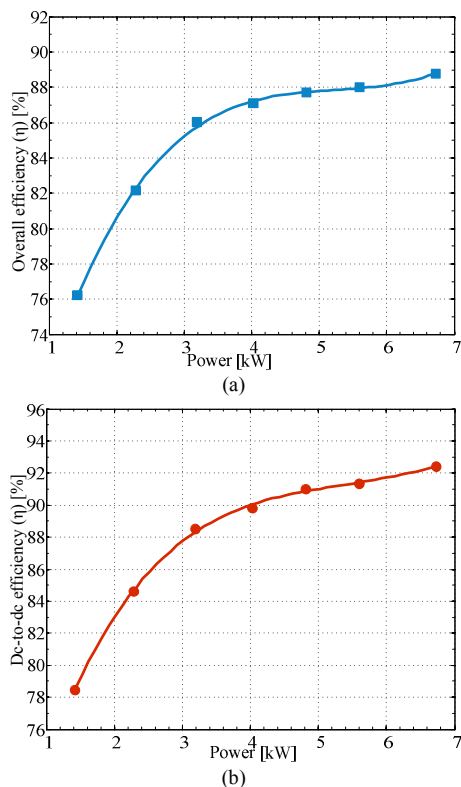Fig. 19. Experimental waveforms for the inverter, transformer, and rectifier outputs.

(a)

(b)

Fig. 20. System efficiency at different power transfer levels for wired operation: Overal efficiency (a) and dc-to-dc efficiency (b).

The integrated charger is tested in wired and wireless modes with different transformer turns-ratios because of the difference in the voltage gain of the resonant tank, the input and output voltage requirements. In order to optimize the design with one single transformer turns-ratio the system had to be tested with 10:2 transformer for the wired mode and 8:5 transformer for the wireless mode. For the wired mode in order to obtain the desired 311 V at the load with the 10:2 transformer, the input dc-link voltage has to be around 1500 V_{rms}. This voltage is above the ratings of the devices being used so this turns-ratio will not be suitable for the wired mode.

However, for the wireless mode the 8:5 turns-ratio will work in both operating modes, wired and wireless, with some reduction in the overall efficiency. This is because the lower turns-ratio will cause an increase in the current from 35 A_{rms} to 58 A_{rms} on the primary side of the transformer for the same output power.

For the repeated tests, the efficiencies are shown in Fig. 21 with 8:5 transformer turns-ratio. The overall efficiency of the system dropped from 85.9% to 84.4% whereas the dc-to-dc efficiency dropped from 88.9% to 87.4%. There is another effect on the overall system performance because of the increase in current. The voltage drop across the leakage inductance of the transformer will be much higher than the previous case because of the increase in current. The leakage inductance for this transformer was 23.4 µH. At the same resonant frequency as in the 10:2 turns-ratio case the drop was less. With the resonant voltage gain considered, the effective turns-ratio is 2.4 instead of 1.6 (8:5).
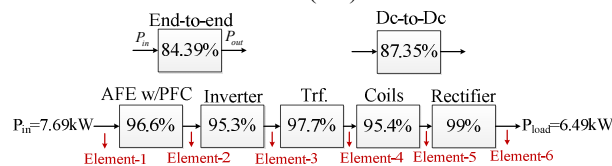

Fig. 21. Stage by stage efficiency for wireless operation with 8:5 transformer turns ration (repeated test).

V. CONCLUSIONS

A new integrated charger topology with wired and wireless charging and boost function is presented. According to the experimental test results, the end-to-end and dc-to-dc efficiencies of the system were 85.9% and 88.9% for wireless charging mode whereas these efficiency values were 88.8% and 92.4% for the wired charging mode of operation. Based on the references performance of commercially available OBCs from manufacturers, Chevy Volt OBC is 89.6% efficient at level-2 and 86.8% efficient at level-1 [22] and Nissan Leaf OBC efficiency is 90.9% at level-2 [23]. The proposed integrated charger, with both the wired and wireless charging functionalities, is on par with the performance of these commercially available units. In order to have the system interoperable with both wired and wireless charging modes, the transformer turns ratio had to be changed to 8:5 instead of 10:2 since the wired option does not have the natural voltage gain effect of the resonant wireless charging. In this case, the same transformer turns ratio provided both wired and wireless charging functionalities without any additional changes in the system but with slight efficiency reduction due to the higher current levels that the primary circuit had to deliver.

REFERENCES

[1] D. Thimmesch, "An SCR inverter with an integral battery charger for electric vehicles," *IEEE Transactions on Industry Applications*, vol. IA-21, no. 4, pp.1023–1029, July/August 1985.

[2] S. –K. Sul and S. J. Lee, "An integral battery charger for electric vehicles," *IEEE Transactions on Industry Applications*, vol. 31, no. 5, pp. 1096-1099, Sept./Oct. 1995.

[3] L. Tang and G. J. Su, "A Low-Cost, Digital-Controlled Charger for Plug-In Hybrid Electric Vehicles," in *Proc., IEEE Energy Conversion Conference & Exposition (ECCE)*, pp. 3923–3929, September 2009, San Jose, CA.

[4] G. J. Su and L. Tang, "An Integrated Onboard Charger and Accessory Power Converter for Plug-in Electric Vehicles," in *Proc., IEEE Energy Conversion Congress and Exposition (ECCE)*, pp. 1592–1597, September 15–19, 2013, Denver, CO.

[5] G. J. Su and L. Tang, "A New Integrated Onboard Charger and Accessory Power Converter for Plug-in Electric Vehicles," in *Proc., IEEE Energy Conversion Congress and Exposition (ECCE)*, pp. 4790–4796, September 2014, Pittsburgh, PA.

[6] G. J. Su and L. Tang, "An integrated onboard charger and accessory power converter using WBG devices," in *Proc., IEEE Energy Conversion Congress and Exposition (ECCE)*, pp. 6306–6313, September 2015, Montreal, Canada.

[7] M. Chinthavali, O. C. Onar, S. L. Campbell, and L. M. Tolbert, "Isolated wired and wireless battery charger with integrated boost converter for PEV applications," in *Proc., IEEE Energy Conversion Congress & Exposition (ECCE)*, pp. 607-614, September 2015, Montreal, Canada.

[8] M. Chinthavali, O. C. Onar, S. L. Campbell, and L. M. Tolbert, "Integrated charger with wireless charging and boost functions for PHEV and EV applications," in *Proc., IEEE Transportation Electtification Conference and Expo, (ITEC)*, pp. 1-8, June 2015, Dearborn, MI.

[9] SAE J2954 Standards Development for Wireless Charging of Electric and Plug-in Hybrid Vehicles, Standard development currently in progress, Available online: http://standards.sae.org/wip/j2954/

[10] W. E. Rippel and A. G. Cocconi, "Integrated motor drive and recharge system," *US Patent 5099186*, March 1992.

[11] D. G. Woo, G. Y. Choe, J. Kim, B. Lee, J. Hur, G. Kang, "Comparison of integrated battery chargers for plug-in electric vehicles: Topology and control," in *Proc. IEEE International Electric Machines & Drives Conference (IEMDC)*, pp. 1294-1299, May 2011, Niagara Falls, CA.

[12] L. Tang and G. J. Su, "A low-cost, digitally-controlled charger for plug-in hybrid electric Vehicles," in *Proc., IEEE Energy Conversion Congress and Exposition (ECCE)*, pp. 3923-3929, September 2009, San Jose, CA.

[13] L. De-Sousa and B. Bouchez, "Method and electric combined device for powering and charging with compensation means," *International Patent WO 2010/057893 A1*, 2010.

[14] S. Haghbin, "An isolated integrated charger for electric or plug-in hybrid vehicles," *Thesis for The Degree of Licentiate of Engineering*, Chalmers University of Technology Göteborg, Sweden, 2011.

[15] A. Bruyère, L. De Sousa, B. Bouchez, P. Sandulescu, X. Kestelyn, and E. Semail, "A Multiphase Traction/Fast-Battery-Charger Drive for Electric or Plug-in Hybrid Vehicles," in *Proc. IEEE Vehicle Power and Propulsion Conference (VPPC)*, pp. 1-7, September 2010, Lille, France.

[16] Y. J. Lee, A. Khaligh, and A. Emadi, "Advanced integrated bidirectional ac/dc and dc/dc converter for plug-in hybrid electric vehicles," *IEEE Transactions on Vehicular Technology*, vol. 58, no. 8, pp. 3970–3980, October 2009.

[17] D. C. Erb, O. C. Onar, and A. Khaligh, "An integrated bidirectional power electronic converter with multi-level AC–DC/DC–AC converter and non-inverted buck-boost converter for PHEVs with minimal grid level disruptions," in *Proc., IEEE Vehicle Power and Propulsion Conference (VPPC)*, pp. 1–6, September 2010, Lille, France.

[18] H. Chen, X. Wang, and A. Khaligh, "A single stage integrated bidirectional ac/dc and dc/dc converter for plug-in hybrid electric vehicles," in *Proc., IEEE Vehicle Power and Propulsion Conference (VPPC)*, pp. 1–6, September 2011, Chicago, IL.

[19] S. Dusmez and A. Khaligh, "A novel low cost integrated on-board charger topology for electric vehicles and plug-in hybrid electric vehicles," in *Proc., Applied Power Electronics Conference and Exposition (APEC)*, pp. 2611–2616, Feburary 2012, Orlando, FL.

[20] M. S. Chinthavali, O. C. Onar, J. M. Miller, and L. Tang, "Single-phase active boost rectifier with power factor correction for wireless power transfer applications," in *Proc., IEEE Energy Conversion Congress and Exposition (ECCE)*, pp. 3258-3265, September 2013, Denver, CO.

[21] J. M. Miller and O. C. Onar, Short Course on Wireless Power Transfer (WPT) Systems, *IEEE Transportation Electrification Conference and Expo (ITEC)*, June 2013, Dearborn, MI.

[22] B. M. Conlon, T. Blohm, M. Harpster, A. Homes, and M. Palardy, "The next generation "Voltec" extended range EV propulsion system," *SAE International Journal of Alternative Powertrains*, vol. 4, no. 2, pp. 1-12, 2015-01-1152, April 2015.

[23] Idaho National Laboratory, "Nissan Leaf – VIN 0356, Advanced Vehicle Testing – Baseline Testing Reults," Available online: http://avt.inel.gov/pdf/fsev/fact2011nissanleaf.pdf